

2D Layered Perovskites

Solution Processable Materials

The recent discovery that single-layer 2D perovskites can be prepared using solution processing techniques¹ has been followed by enormous research into optoelectronic applications of 2D perovskites including light emitting diodes (LEDs),² phototransistors,³ and solar cells.⁴

Tunable Emission Wavelength

Photoluminescent 2D perovskites have an emission wavelength that changes depending on the layer thickness and the choice of amine and halide. We offer an excellent portfolio of the most popular 2D perovskite compositions for photoluminescence based devices.

Improved Moisture Stability

Solar cells fabricated with 2D perovskites have improved stability in moist air compared to 3D perovskites.⁴



| Formula | Cat. No. | Layer Thickness | $(\text{RNH}_3)_2(\text{MeNH}_2)_{n-1}\text{Pb}_n\text{X}_{3n+1}$ | | |
|--|----------|-----------------|---|----|---|
| | | | R | X | n |
| $(\text{BA})_2\text{PbI}_4$ | 910961 | n=1 | Bu | I | 1 |
| $(\text{BA})_2\text{PbBr}_4$ | 910953 | n=1 | Bu | Br | 1 |
| $(\text{PEA})_2\text{PbI}_4$ | 910937 | n=1 | PE | I | 1 |
| $(\text{PEA})_2\text{PbBr}_4$ | 910945 | n=1 | PE | Br | 1 |
| $(\text{BA})_2(\text{MA})\text{Pb}_2\text{I}_7$ | 912816 | n=2 | Bu | I | 2 |
| $(\text{BA})_2(\text{MA})_2\text{Pb}_3\text{I}_{10}$ | 912557 | n=3 | Bu | I | 3 |
| $(\text{BA})_2(\text{MA})_3\text{Pb}_4\text{I}_{13}$ | 914363 | n=4 | Bu | I | 4 |
| $(\text{BA})_2(\text{MA})_4\text{Pb}_5\text{I}_{16}$ | 912301 | n=5 | Bu | I | 5 |

BA = n-butylammonium; PEA = 2-phenylethylammonium; MA = methylammonium, Bu=n-butyl, PE=2-phenylethyl

References:

- 1) Dou, L.; Wong, A. B.; Yu, Y.; Lai, M.; Kornienko, N.; Eaton, S. W.; Fu, A.; Bischak, C. G.; Ma, J.; Ding, T.; Ginsberg, N. S.; Wang, L.-W.; Alivisatos, A. P.; Yang, P. *Science* **2015**, *349*, 1518. DOI: 10.1126/science.aac7660
- 2) Yuan, M.; Quan, L. N.; Comin, R.; Walters, G.; Sabatini, R.; Voznyy, O.; Hoogland, S.; Zhao, Y.; Beauregard, E. M.; Kanjanaboos, P.; Lu, Z.; Kim, D. H.; Sargent, E. H. *Nat. Nanotechnol.* **2016**, *11*, 872. DOI: 10.1038/NNANO.2016.110
- 3) Shao, Y.; Liu, Y.; Chen, X.; Chen, C.; Sarpkaya, I.; Chen, Z.; Fang, Y.; Kong, J.; Watanabe, K.; Taniguchi, T.; Taylor, A.; Huang, J.; Xia, F. *Nano Lett.* **2017**, *17*, 7330. DOI: 10.1021/acs.nanolett.7b02980
- 4) Cao, D. H.; Stoumpos, C. C.; Farha, O. K.; Hupp, J. T.; Kanatzidis, M. G. *J. Am. Chem. Soc.* **2015**, *137*, 7843. DOI: 10.1021/jacs.5b03796

SigmaAldrich.com/perovskite

The Life Science business of Merck operates as MilliporeSigma in the U.S. and Canada.

© 2022 Merck KGaA, Darmstadt, Germany and/or its affiliates. All Rights Reserved. Merck, the vibrant M, and Sigma-Aldrich are trademarks of Merck KGaA, Darmstadt, Germany or its affiliates. All other trademarks are the property of their respective owners. Detailed information on trademarks is available via publicly accessible resources.

MK_AD9822EN 43729 09/2022

The Life Science business of Merck operates as MilliporeSigma in the U.S. and Canada.

Sigma-Aldrich[®]
Lab & Production Materials

Manipulating Charge Transfer and Transport via Intermediary Electron Acceptor Channels Enables 19.3% Efficiency Organic Photovoltaics

Lingling Zhan,* Shuixing Li, Yaokai Li, Rui Sun, Jie Min, Yiyao Chen, Jin Fang, Chang-Qi Ma, Guanqing Zhou, Haiming Zhu, Lijian Zuo, Huayu Qiu, Shouchun Yin,* and Hongzheng Chen*

Balancing and improving the open-circuit voltage (V_{oc}) and short-circuit current density (J_{sc}) synergistically has always been the critical point for organic photovoltaics (OPVs) to achieve high efficiencies. Here, this work adopts a ternary strategy to regulate the trade-off between V_{oc} and J_{sc} by combining the symmetric-asymmetric non-fullerene acceptors that differ at terminals and alkyl side chains to build the ternary OPV (TOPV). It is noticed that the reduced energy disorder and the enhanced luminescence efficiency of TOPV enable a mitigated energy loss and a higher V_{oc} . Meanwhile, the third component, which is distributed at the host donor–acceptor interface, acts as the charge transport channel. The prolonged exciton lifetime, the boosted charge mobility, and the depressed charge recombination promote the TOPV to obtain an improved J_{sc} . Finally, with synergistically improved V_{oc} and J_{sc} , the TOPV delivers an optimal efficiency of 19.26% (certified as 19.12%), representing one of the highest values reported so far.

Y-serious acceptors and the multi-components strategy, the power conversion efficiencies (PCEs) of the single-junction OPVs have already reached 19%,^[19,20] with the best fill factors (FFs) exceeding 80%.^[21,22] However, the trade-off between the open-circuit voltage (V_{oc}) and the short-circuit current density (J_{sc}) still remains as a challenge to handle with in OPV devices.^[23–27] Therefore, the synergistic improvement of V_{oc} and J_{sc} will be attractive for marching the efficiencies further for OPVs.^[28–30]

The charge transfer (CT) state cannot only affect the energy loss (E_{loss}) but also the generation efficiency of photo-induced carriers.^[26] Narrowing the offset (ΔE_{LE-CT}) between the energy level of the CT state (E_{CT}) and the lowest excited state (E_{LE}) may reduce the probability of excitons

quenching back to the ground state, which helps in mitigating E_{loss} for a higher V_{oc} . However, the diminished driving force is not in favor of exciton dissociation for a higher J_{sc} , and vice versa.^[29] The properties of CT states at the donor–acceptor (D–A) interfaces are supposed to be affected by the morphology

1. Introduction

Organic photovoltaics (OPVs) have been rapidly advanced, benefitted from the novelty of materials,^[1–9] and intelligent device engineering.^[10–18] Especially based on the exquisite designed

L. Zhan, H. Qiu, S. Yin
Key Laboratory of Organosilicon Chemistry and Materials Technology
of Ministry of Education
College of Material
Chemistry and Chemical Engineering
Hangzhou Normal University
Hangzhou 311121, P. R. China
E-mail: linglingzhan@hznu.edu.cn; yinsc@hznu.edu.cn


L. Zhan, S. Li, Y. Li, L. Zuo, H. Chen
State Key Laboratory of Silicon Materials
MOE Key Laboratory of Macromolecular Synthesis and Functionalization
International Research Center for X Polymers
Department of Polymer Science and Engineering
Zhejiang University
Hangzhou 310027, P. R. China
E-mail: hzchen@zju.edu.cn

R. Sun, J. Min
The Institute for Advanced Studies
Wuhan University
Wuhan 430072, P. R. China

Y. Chen
Vacuum Interconnected Nanotech Workstation (Nano-X)
Suzhou Institute of Nano-Tech and
Nano-Bionics
Chinese Academy of Sciences (CAS)
Suzhou 215123, P. R. China

J. Fang, C.-Q. Ma
i-Lab & Printable Electronics Research Centre
Suzhou Institute of Nano-Tech and Nano-Bionics
Chinese Academy of Sciences (CAS)
Suzhou 215123, P. R. China

G. Zhou, H. Zhu
Department of Chemistry
Zhejiang University
Hangzhou 310027, P. R. China

 The ORCID identification number(s) for the author(s) of this article can be found under <https://doi.org/10.1002/aenm.202201076>.

DOI: 10.1002/aenm.202201076

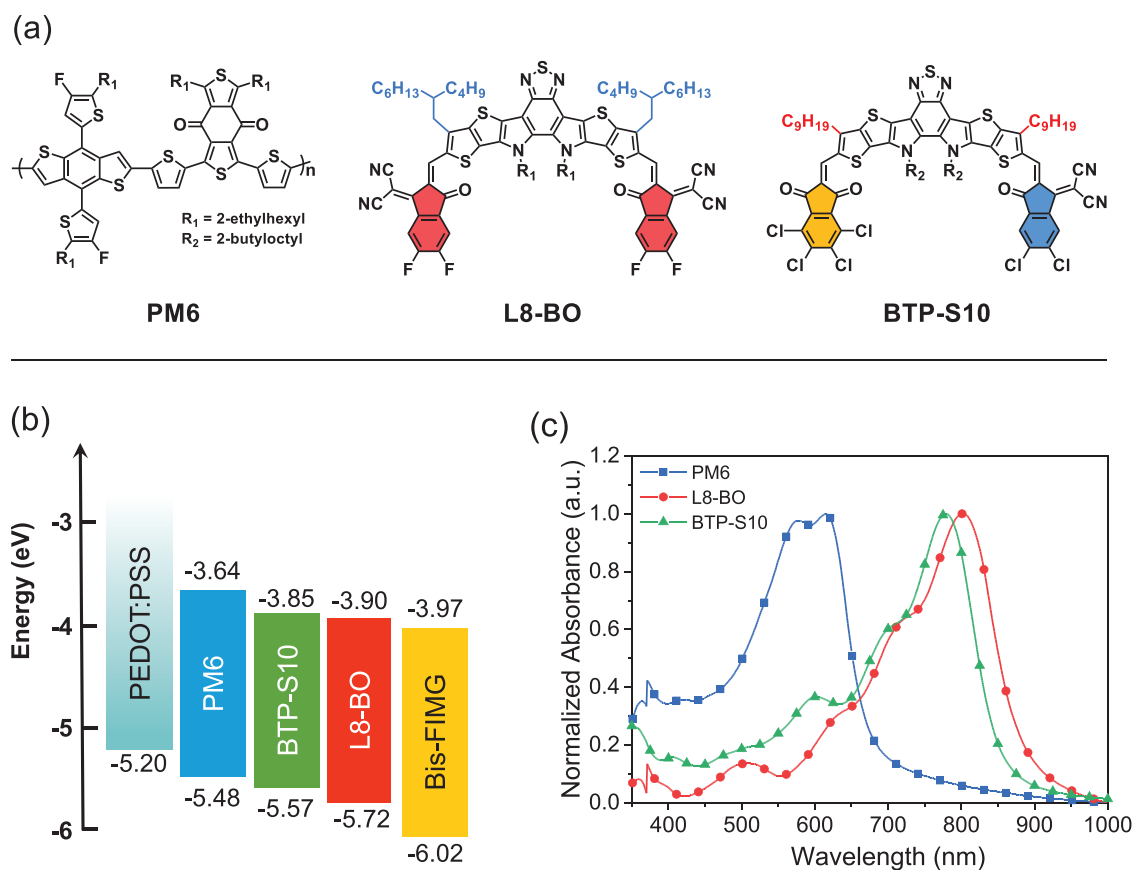


Figure 1. a) Chemical structure of PM6, L8-BO, and BTP-S10. b) Energy diagram of PM6, L8-BO, and BTP-S10 determined by CV measurements. c) Normalized UV spectra of neat films.

of the active layer,^[31–33] while ternary OPV (TOPV) is proven to be an effective way for energy level regulation and morphology optimization.^[18,34,35] For designing efficient TOPVs, if the third component helps upshift the E_{CT} in TOPV, we can expect the mitigated non-radiative recombination process for acquiring a reduced energy loss (E_{loss}).^[36] On the other hand, if the third component locates at the host D-A interfaces, the generated extra charge transport channels can help exciton dissociation, thus counteracting the deficiency of reduced driving force arising from lifted CT state, and enabling high J_{sc} for pursuing a breakthrough in efficiency.^[37,38]

The surface energy difference between materials acts as the dominant factor for determining the position of the third component in the blends.^[21,38] The third component with a more obvious surface energy difference to the host D or A, representing weaker compatibility, is believed to locate at the host D/A interface more easily.^[39–41] With the above thoughts, we here select symmetric-asymmetric non-fullerene acceptors (NFAs) with different terminals and alkyl side chains to construct the TOPV. The symmetric L8-BO has good compatibility with PM6,^[42] while the newly synthesized asymmetric BTP-S10 bearing six chlorine atoms shows weak compatibility with PM6, which makes BTP-S10 mainly located at the host D/A interfaces for working as extra charge transport channels. It's also found that the diminished ΔE_{LE-CT} and enhanced luminescence efficiency of TOPV contribute to the lower E_{loss} and

the higher V_{oc} .^[43] Besides, the prolonged exciton lifetime, the boosted charge mobility, and the depressed charge recombination are observed in TOPVs, thus benefiting the increase of J_{sc} in TOPVs. As a result, TOPV based on PM6:L8-BO:BTP-S10 delivers a champion efficiency of 19.26% (certified as 19.12%) with an increased V_{oc} of 0.898 V, an improved J_{sc} of 26.80 mA cm⁻², and a high FF of 80.22%, which represents one of the highest efficiencies reported to date. This work provides a workable ternary design for synergistically boosting V_{oc} and J_{sc} , thus pursuing higher efficiencies.

2. Results and Discussion

2.1. Synthesis and Characterization

Figure 1a shows the chemical structures of polymer donor PM6, symmetric acceptor L8-BO, and newly synthesized asymmetric acceptor BTP-S10. The synthetic details of BTP-S10 can be found in Supporting Information with basic material properties shown in Figures S1–S4, Supporting Information. L8-BO is an efficient NFA reported by Sun et al. with two branched alkyl side chains on the β -position of thiophene rings, enabling improved molecular packing for high FF over 80% and high PCE over 18%. However, it can be aware that the E_{loss} (0.55 eV) is still a bit high, and the active layer is also a bit thin, thus

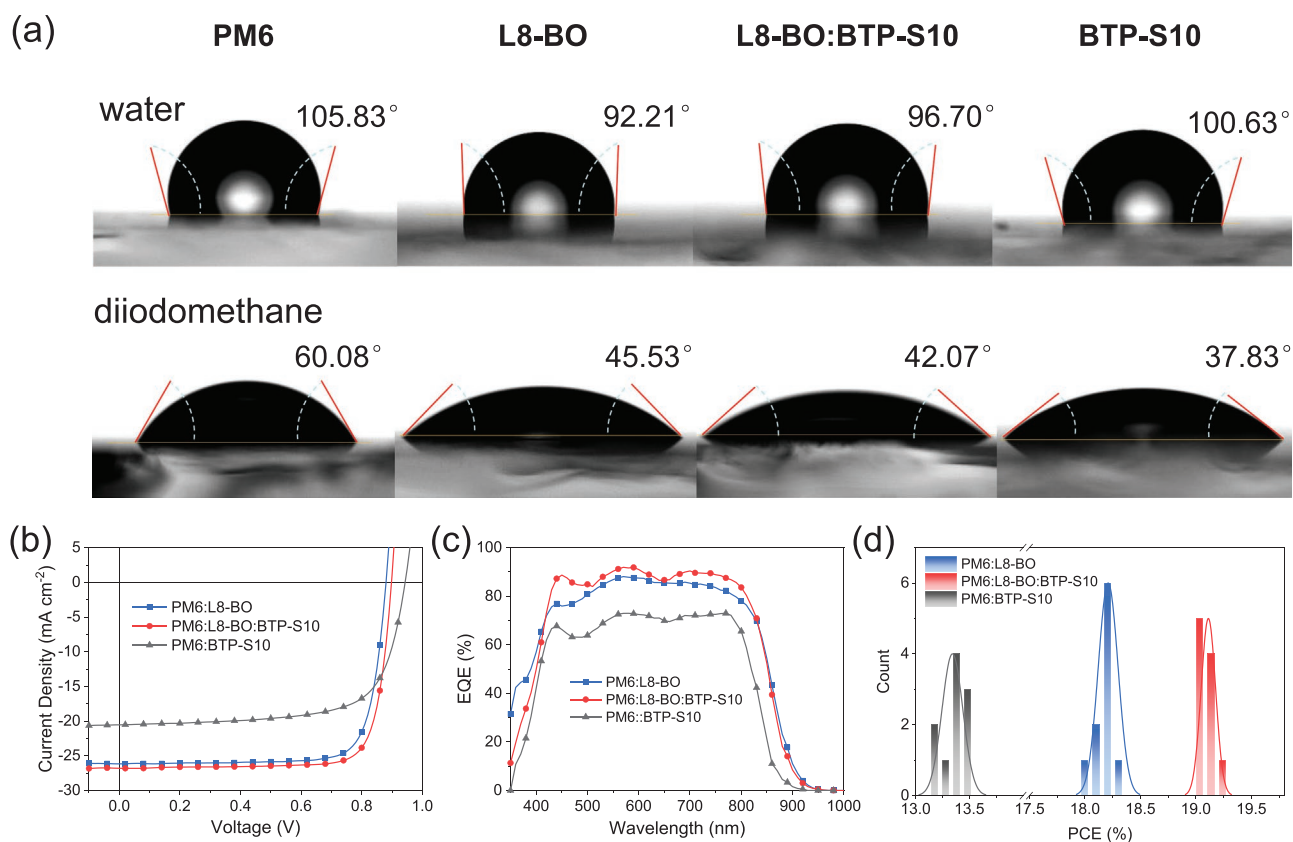


Figure 2. a) Contact angle images of PM6, L8-BO, L8-BO:BTP-S10, BTP-S10 films with water and diiodomethane droplet on top. b) $J-V$ curves of PM6:L8-BO:BTP-S10 OPVs with different weight ratios of BTP-S10. c) EQE curves of the corresponding devices with different weight ratios of BTP-S10. d) Statistical PCE variations with the change of BTP-S10 ratio.

limiting the V_{oc} and J_{sc} values for the PM6:L8-BO system. To enable a lower E_{loss} and higher photovoltaic performance, the designed third component should be the one with higher luminescence efficiency and also lower miscibility with the polymer donor.^[15,41] Based on these considerations, BTP-S10 is designed with maximal six chlorine atoms at the terminals for enhancing emission, an asymmetric configuration and two shorter linear alkyl side chains on the β -position of thiophene rings for reducing miscibility with polymer donor.^[43] The resulting BTP-S10 possesses a lowest unoccupied molecular orbital (LUMO) level of -3.85 eV and a highest occupied molecular orbital (HOMO) level of -5.57 eV, deep enough for pairing with PM6. Removing the cyano-group on one side reduces the quinoid resonance effect, thus blue-shifting the absorption of BTP-S10, relative to that of L8-BO.

Contact angle experiments were performed to check the miscibility situations (Figure 2a and Table S1, Supporting Information) and get the Flory–Huggins interaction parameter χ .^[44] The smaller χ^{D-A} it is, the better miscibility it is, and vice versa.^[45,46] The value of χ^{D-A} between PM6 and BTP-S10 is calculated as 2.153, while only 0.473 between PM6 and L8-BO, certifying the significantly reduced miscibility between PM6 and designed BTP-S10. After 20% (by wt) BTP-S10 is introduced, the obtained L8-BO:BTP-S10 composite shows an increased χ^{D-A} of 1.121, indicating BTP-S10 is effective in tuning the miscibility between donor and acceptor.

To figure out where the introduced BTP-S10 locates in the ternary system (D:A₁:A₂), the wetting coefficient (ω) of the third component A₂ in the mixture of D:A₁ is calculated according to Young's equation:^[47]

$$\omega_{A_2} = \frac{\gamma_{A_1/A_2} - \gamma_{D/A_2}}{\gamma_{D/A_1}} \quad (1)$$

where γ_{A_1/A_2} means the interfacial tension between A₁ and A₂, and can be calculated using Wu's Equation:^[47]

$$\gamma_{A_1/A_2} = \gamma_{A_1} + \gamma_{A_2} - 4 \left(\frac{\gamma_{A_1}^d \gamma_{A_2}^d}{\gamma_{A_1}^p + \gamma_{A_2}^p} + \frac{\gamma_{A_1}^p \gamma_{A_2}^p}{\gamma_{A_1}^d + \gamma_{A_2}^d} \right) \quad (2)$$

The γ_A^d and γ_A^p are the dispersion and polar components of γ_A . The calculated interfacial tension $\gamma_{L8-BO/BTP-S10}$, $\gamma_{PM6/L8-BO}$, and $\gamma_{PM6/BTP-S10}$ are 2.77, 1.62, and 4.63 mN m⁻¹, respectively. Component A₂ will lie in the phase of component D if the wetting coefficient is larger than 1 ($\omega_{A_2} > 1$), but in the domain of component A₁ if $\omega_{A_2} < -1$. If $-1 < \omega_{A_2} < 1$, then component A₂ will be located at the interfaces of D and A₁.^[47] For PM6:L8-BO:BTP-S10 ternary blend, the $\omega_{BTP-S10}$ is calculated as -0.98 (Table S1, Supporting Information), confirming that BTP-S10 is located at the interfaces between PM6 and L8-BO. The BTP-S10 component in the sandwich structure of blend can work as channels for boosting exciton dissociation and

Table 1. The performance parameters of the champion devices based on PM6:L8-BO:BTP-S10 with different BTP-S10 contents.

| BTP-S10 ratio [%] | V_{oc} [V] | J_{sc} [mA cm^{-2}] | $J_{cal.}$ [mA cm^{-2}] ^{a)} | FF [%] | PCE [%] ^{b)} |
|-------------------|-----------------------|----------------------------------|--|----------------------|-----------------------|
| 0 | 0.880 (0.877 ± 0.003) | 26.16 (26.24 ± 0.26) | 25.35 | 79.34 (79.12 ± 0.73) | 18.30 (18.21 ± 0.08) |
| 20 | 0.898 (0.902 ± 0.004) | 26.80 (26.59 ± 0.14) | 26.19 | 80.22 (79.87 ± 0.24) | 19.26 (19.11 ± 0.06) |
| 100 | 0.943 (0.947 ± 0.003) | 20.54 (20.54 ± 0.13) | 19.93 | 69.46 (68.74 ± 0.94) | 13.44 (13.34 ± 0.09) |
| 20 ^{c)} | 0.892 | 26.88 | | 79.73 | 19.12 |

^{a)}Integrated current densities from EQE curves; ^{b)}Average PCEs from 10 devices; ^{c)}Certified results from National PV Industry Measurement and Testing Center (NPVIM).

charge transport, thus helping improve the J_{sc} of TOPVs as proven below.

2.2. Photovoltaic Characteristics

The conventional device structure of indium tin oxide (ITO)/poly(3,4-ethylenedioxythiophene) poly(styrene sulfonate) (PEDOT:PSS)/active layer/bisfulleropyrrolidinium tris(methoxyethoxy) phenyl iodide (Bis-FIMG)/Ag was applied to fabricate OPVs for evaluating photovoltaic performances. Fabrication details are described in Supporting Information. Figure 2b shows the J - V curves of the optimal binary and ternary devices and relevant photovoltaic parameters are summarized in **Table 1** (the original parameters of various devices are listed in Table S2, Supporting Information). For PM6:L8-BO binary OPV, the performance is found to be a PCE of 18.30%, with a V_{oc} of 0.880 V, a J_{sc} of 26.16 mA cm^{-2} , and a FF of 79.34%. For PM6:BTP-S10 binary OPV, it delivers a PCE of 13.44% with a high V_{oc} of 0.943 V, a J_{sc} of 20.54 mA cm^{-2} , and a FF of 69.46%. Obviously, PM6:BTP-S10 binary system shows a significantly superiority in voltage, providing great possibility in enhancing the voltage of TOPVs by adding BTP-S10 as the third component. As expected, with increasing the weight ratios of BTP-S10 in ternary blends, a gradual increase in V_{oc} can be observed (Table S4, Supporting Information), and the optimal PCE of TOPVs is achieved with 20% BTP-S10 ratio. The champion TOPV exhibits an outstanding PCE of 19.26% with a V_{oc} of 0.898 V, a J_{sc} of 26.80 mA cm^{-2} , and a FF of 80.22%. Relative to PM6:BTP-S10 binary system, all three device parameters, especially V_{oc} and J_{sc} , are improved in TOPVs, certifying the success of utilizing BTP-S10 as the third component to optimize voltage and photocurrent as intended design purpose. The statistical results of PCE variations for binary and ternary devices also confirm the effectiveness of the ternary strategy (Figure 2d). In order to verify the efficiency reliability, 40 individual ternary devices based on PM6:L8-BO:BTP-S10 blend are fabricated and tested (Figure S5, Supporting Information). The efficiencies of most devices are lying around 19%, confirming the effectiveness of this ternary system. Moreover, the champion TOPV was also sent to the National PV Industry Measurement and Testing Center (NPVIM) for certification, and a certified PCE of 19.12% (V_{oc} = 0.892 V, J_{sc} = 26.88 mA cm^{-2} , and FF = 79.73%) was achieved (Table 1 and Figure S6, Supporting Information).

The EQE spectra of relevant devices are shown in Figure 2c. The addition of BTP-S10 will lead to a tiny blue-shifted absorption edge, but bring obvious benefits in sharper edge and higher EQE values in the broad range of \approx 400–850 nm for TOPV, thus

being responsible for the J_{sc} enhancement as detected in J - V curve. The calculated $J_{cal.}$ values of the devices from the EQE curves are consistent with the measured J_{sc} values in the J - V curves with the errors less than 3% (Table 1). To confirm the high EQE response, we measured and calculated the IQE of the optimal ternary device (Figure S7, Supporting Information). The parasitic absorption spectrum could be calculated by $1 - R_1$, and the total absorption spectrum of the ternary device could be calculated by $1 - R_2$, where R_1 is the reflection spectrum of the ternary device without active layer and the R_2 is the reflection spectrum of the whole ternary device. So, the total absorption of the active layer could be calculated by minusing the parasitic absorption from the absorption of the whole device. In other words, $Abs = (1 - R_2) - (1 - R_1) = R_1 - R_2$.^[48] As calculated by the equation: $IQE = EQE/Abs = EQE/(R_1 - R_2)$, and corresponding IQE spectra are shown in Figure S7, Supporting Information. In the wavelength range from 450 to 850 nm, the ternary device displays high IQE value, indicating the efficient photo-current conversion and slight charge recombination in the optimized ternary system.

2.3. Energy Loss

To explain the variation in voltage for TOPVs, we carried out a detailed analysis of the E_{loss} for the binary and ternary OPVs, which can be quantified as the following formula:^[49]

$$E_{loss} = E_g - qV_{oc} = (E_g - qV_{oc}^{SQ}) + (qV_{oc}^{SQ} - qV_{oc}^{rad}) + (qV_{oc}^{rad} - qV_{oc}) \\ = (E_g - qV_{oc}^{SQ}) + q\Delta V_{oc}^{rad, below\ gap} + q\Delta V_{oc}^{non-rad} = \Delta E_1 + \Delta E_2 + \Delta E_3 \quad (3)$$

where E_g is the band-gap, V_{oc}^{SQ} is the maximum V_{oc} under the SQ limit, and ΔV_{oc}^{rad} is the V_{oc} when only radiative recombination is considered. We determined the E_g value by the derivatives of the Fourier transform photocurrent spectroscopy (FTPS)-EQE curve and then calculated with the following equation:^[50]

$$E_g = \frac{\int_a^b E_g P(E_g) dE_g}{\int_a^b P(E_g) dE_g} \quad (4)$$

where the integration limits a and b are chosen as the $P(a) = P(b) = 0.5\text{Max}[P(E_g)]$ (Figure S8, Supporting Information). ΔE_1 is an unavoidable part. ΔE_2 is the part affected by the blends' reorganization energy and energy disorder degree. For ΔE_3 , it has a quantitative relationship with the luminescence efficiency

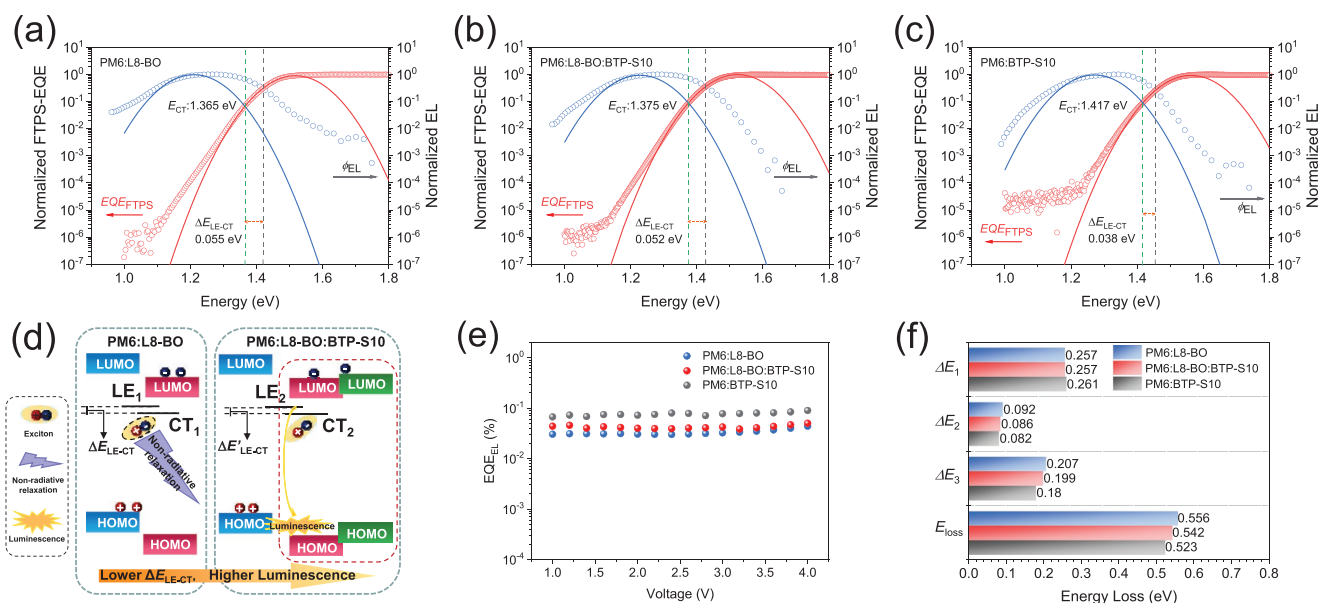


Figure 3. Gaussian fits of FTPS-EQE and EL curves via Marcus equation for devices based on a) PM6:L8-BO, b) PM6:L8-BO:BTP-S10, and c) PM6:BTP-S10 blend. d) A schematic diagram of energy levels of the CT and LE states, and relevant ΔE_{LE-CT} for host binary system and ternary system (CT_1 , LE_1 , $\Delta E'_{LE-CT}$, CT_2 , LE_2 , and $\Delta E'_{LE-CT}$ represents the CT state, LE state, and their energy offset of PM6:L8-BO and ternary blend, respectively). e) EQE_{EL} of corresponding OPVs at various bias voltages. f) Comparison of ΔE_1 , ΔE_2 , and ΔE_3 values and E_{loss} .

of photovoltaic materials, which can be expressed as the following formula:^[50]

$$\Delta E_3 = q \Delta V_{oc}^{non-rad} = -kT \ln(EQE_{EL}) \quad (5)$$

where k is the Boltzmann constant, T is the Kelvin temperature, and EQE_{EL} is the electroluminescence quantum efficiency of the device. The characterization method for calculating E_{loss} is shown in Figure 3 and Figure S9, Supporting Information, and the calculated detailed E_{loss} is shown in Table 2. It is found that the bandgap of TOPV is negligibly affected, but the E_{loss} is reduced to 0.542 eV, thus enabling a higher V_{oc} than relevant binary OPV based on PM6:L8-BO ($E_{loss} = 0.556$ eV). Binary OPV based on PM6:BTP-S10 shows the lowest E_{loss} of 0.523 eV, verifying BTP-S10 as a low-energy-loss material as intended design strategy. The reduction of E_{loss} for TOPV is the result of both mitigation of ΔE_2 and ΔE_3 , benefitted from BTP-S10.

By examining electroluminescence spectroscopy (EL) and high-resolution Fourier transform photocurrent spectroscopy EQE spectra (FTPS-EQE), we find that the decrease in ΔE_2 in

TOPV is possibly related to the degree of energy disorder. The degree of the energy disorder can be quantified by an Urbach energy parameter (E_U), which follows Urbach's rule as follows:^[6]

$$\alpha(E) = \alpha_0 e^{\frac{E-E_0}{E_U}} \quad (6)$$

In the formula, $\alpha(E)$ is the absorption coefficient, α_0 and E_0 , are two constants, and E is the photon energy. A smaller E_U indicates a lower energy disorder. By fitting FTPS-EQE curves according to Equation (5), E_U values are found to be 27.27 meV for PM6:L8-BO OPV, 25.71 meV for TOPV, and 25.40 meV for PM6:BTP-S10 OPV (Figure S9, Supporting Information). The reduction in E_U confirms the effect of energy disorder mitigation on ΔE_2 for TOPV, which is consistent well with the sharper EQE edges of the TOPV, as mentioned above.

For analyzing the ΔE_3 , we detected and compared the binary and ternary devices' CT states and their luminescence efficiencies.^[51] E_{CT} can be extracted by performing Gaussian fits on highly sensitive EQE and EL in the spectral range of charge transfer (CT) absorption with the Marcus equations:^[52]

Table 2. Detailed energy losses of OPVs based on PM6:L8-BO:BTP-S10 with different BTP-S10 contents.

| BTP-S10 ratio [%] | E_g [eV] | qV_{oc} [eV] | qV_{oc}^{SQ} [eV] | qV_{oc}^{rad} [eV] | ΔE_1 [eV] | ΔE_2 [eV] | ΔE_3 [eV] | E_{loss} [eV] | Exp. $q \Delta V_{oc}^{non-rad}$ [eV] | $EQE_{EL}^{a)}$ ($\times 10^{-2}\%$) |
|-------------------|------------|----------------|---------------------|----------------------|-------------------|-------------------|-------------------|-----------------|---------------------------------------|--|
| 0 | 1.440 | 0.884 | 1.183 | 1.091 | 0.257 | 0.092 | 0.207 | 0.556 | 0.208 | 3.30 (3.40 \pm 0.10) |
| 20 | 1.441 | 0.899 | 1.184 | 1.097 | 0.257 | 0.086 | 0.199 | 0.542 | 0.201 | 4.22 (4.24 \pm 0.03) |
| 100 | 1.475 | 0.952 | 1.214 | 1.132 | 0.261 | 0.082 | 0.180 | 0.523 | 0.185 | 7.64 (7.53 \pm 0.05) |

^{a)}The value in parentheses is the average EQE_{EL} from three devices.

$$EQE_{PV}(E) = \frac{f_j}{E\sqrt{4\pi\lambda_j kT}} \exp\left(-\frac{(E_{CT} + \lambda_j - E)^2}{4\lambda_j kT}\right) \quad (7)$$

and

$$EQE_{EL}(E) = \frac{Ef_j}{\sqrt{4\pi\lambda_j kT}} \exp\left(-\frac{(E_{CT} - \lambda_j - E)^2}{4\lambda_j kT}\right) \quad (8)$$

where λ_j is the reorganization energy; f_j is the electronic coupling (transfer integral) between states. The results of Gaussian fits are shown in Figure 3a–c. The E_{CT} value is found to be 1.365 eV for PM6:L8-BO, 1.375 eV for PM6:L8-BO:BTP-S10, and 1.417 eV for PM6:BTP-S10-based devices, respectively. Then, with the E_{LE} values (1.420, 1.427, and 1.455 eV, for PM6:L8-BO, PM6:L8-BO:BTP-S10, and PM6:BTP-S10 devices, respectively),^[36] the energy offset (ΔE_{LE-CT}) between E_{CT} and E_{LE} is calculated as 55 meV for PM6:L8-BO, 52 meV for PM6:L8-BO:BTP-S10, and 38 meV for PM6:BTP-S10-based devices, respectively. Figure 3d shows a schematic diagram of the CT and LE states and relevant ΔE_{LE-CT} for the host binary and ternary systems. The reduced ΔE_{LE-CT} facilitates the excitons transfer from the CT state back to the LE state,^[53] which may mitigate the non-radiative relaxation and boost the luminescence efficiency, and partly decrease the non-radiative recombination.^[54]

As shown in Figure 3e, the PM6:BTP-S10 device has the highest EQE_{EL} of $7.64 \times 10^{-2}\%$, which is over two times than that of the PM6:L8-BO device ($3.30 \times 10^{-2}\%$). For TOPV, the EQE_{EL} is measured as $4.22 \times 10^{-2}\%$. The enhanced luminescence efficiency of TOPV results in a reduction in the ΔE_3 . The above results indicate that the enhanced luminescence efficiency of TOPV is partly caused by the reduced ΔE_{LE-CT} and partly derived from the high ELQY of the BTP-S10-based device, which is in accordance with the EL results and could explain well the reduced non-radiative recombination loss (ΔE_3) in the ternary device.

Finally, due to both mitigations of ΔE_2 and ΔE_3 , TOPVs show a lower E_{loss} , thus enabling an increased voltage. Therefore, our ternary strategy can effectively reduce E_{loss} by mitigating both radiative and non-radiative combination loss.

2.4. Behaviors of Excitons and Charges

We study the effect of symmetric–asymmetric ternary strategy on the dynamic behavior of carriers in the photon–electron process and precisely analyze the behaviors of charge generation (or exciton separation), transport, and recombination. The charge separation of the three blends was investigated using the transient absorption spectroscopy (TAS) technique. Here, we only focus on hole transfer kinetics, since the LUMO offset is large enough to maintain efficient electron transfer for these three OPV systems. 800 nm laser is used to selectively excite NFAs. For neat acceptor film, L8-BO shows pronounced bleaching peaks at ≈ 630 , ≈ 720 , and ≈ 810 nm (Figures S10 and S11, Supporting Information). As comparison, BTP-S10 has obvious bleaching peaks at ≈ 690 and ≈ 760 nm. For the L8-BO:BTP-S10

blend, the bleaching peaks resembles those observed in L8-BO film. For the D:A blends, the corresponding photo-bleaching peaks from acceptors appear immediately after photo-excitation (Figure 4a,b). Then, with the decay of TA signals from acceptors, a new bleaching peak appears at ≈ 640 nm, which is consistent with the absorption feature of PM6 and represents the hole transfer from the acceptor to donor. The hole transfer kinetics are then extracted and shown in Figure 4c, in which the early-stage dynamics with a linear scale, and the region of late-stage with a logarithmic scale, shows more reasonable for the analysis of hole transfer dynamic.^[55] The real hole transfer rate in blend films can be calculated to be by $k_{HT} = k_r - k_0$, where $k_r = \frac{1}{\tau_r}$, and $k_0 = \frac{1}{\tau_0}$, τ_0 is the lifetime of neat acceptor with single exponential fitting and τ_r is the rising time of bleach of PM6 with single exponential fitting. Then, we can obtain the real hole transfer time (τ_i) as 8.48 ps for 0% device, 9.74 ps for 20% device, and 10.58 ps for 100% device, fast enough for achieving efficient charge separation (Figure 4d). Overall, the interfacial charge transfer rates are fast for all three OPV blends under similar conditions, demonstrating that charge separation is unaffected when reducing the V_{oc} loss with ternary strategy.

Time-resolve photoluminescence spectra (TRPL) (Figure 4e) were carried out to analyze OPVs' exciton lifetime and dissociation behavior. The fluorescence lifetime of PM6:L8-BO blend is the lowest ($\tau = 79$ ps), demonstrating that the excitons dissociate faster in this binary system, which is consistent with its lower CT state. Another binary blend of PM6:BTP-S10 possesses a τ of 94 ps, consisted with the higher CT state. Moreover, an improved exciton lifetime of 86 ps is observed for the ternary blend, relative to the PM6:L8-BO binary one, which provides a possibility for the ternary blend exhibiting partly enlarged domains for higher carrier mobility and achieving less charge recombination.

The space charge limited current (SCLC) method was applied to measure the charge transport properties of OPVs. The results are shown in Figure 4f and Figure S13 and Table S4, Supporting Information. For the hole mobility (μ_h), the values for devices based on PM6:L8-BO, PM6:BTP-S10, and PM6:L8-BO:BTP-S10 blends are measured as 9.41×10^{-4} , 8.85×10^{-4} , and $9.72 \times 10^{-4} \text{ cm}^2 \text{ V}^{-1} \text{ s}^{-1}$. For the electron mobility (μ_e), the PM6:L8-BO:BTP-S10 device demonstrates an improved value of $4.13 \times 10^{-4} \text{ cm}^2 \text{ V}^{-1} \text{ s}^{-1}$, relative to those of PM6:L8-BO ($2.34 \times 10^{-4} \text{ cm}^2 \text{ V}^{-1} \text{ s}^{-1}$) and PM6:BTP-S10 ($0.37 \times 10^{-4} \text{ cm}^2 \text{ V}^{-1} \text{ s}^{-1}$) binary devices. Therefore, TOPV presents the highest hole and electron mobility, and more balanced hole/electron mobility ratio, thus beneficial for the enhancement in J_{sc} and FF.

The charge recombination of OPVs is analyzed by measuring $J-V$ curves under various light intensities (P_{light}). The relationship between V_{oc} and P_{light} can be described as $V_{oc} \propto nkT/eln(P_{light})$, where e , k , and T are elementary charge, Boltzmann constant, and temperature in Kelvin, respectively. As shown in Figure S12a, Supporting Information, the slopes of PM6:L8-BO, PM6:L8-BO:BTP-S10, and PM6:BTP-S10 OPVs are 1.12, 1.01, and 1.04 $kT e^{-1}$, respectively, which indicates that monomolecular recombination is well hindered in TOPV. The correlation study between J_{sc} and P_{light} ($J_{sc} \propto P_{light}$) shows that the bimolecular recombination of the TOPV presents a similar situation as that of PM6:L8-BO binary device (Figure S12b, Supporting Information). Anyway, charge recombination situation

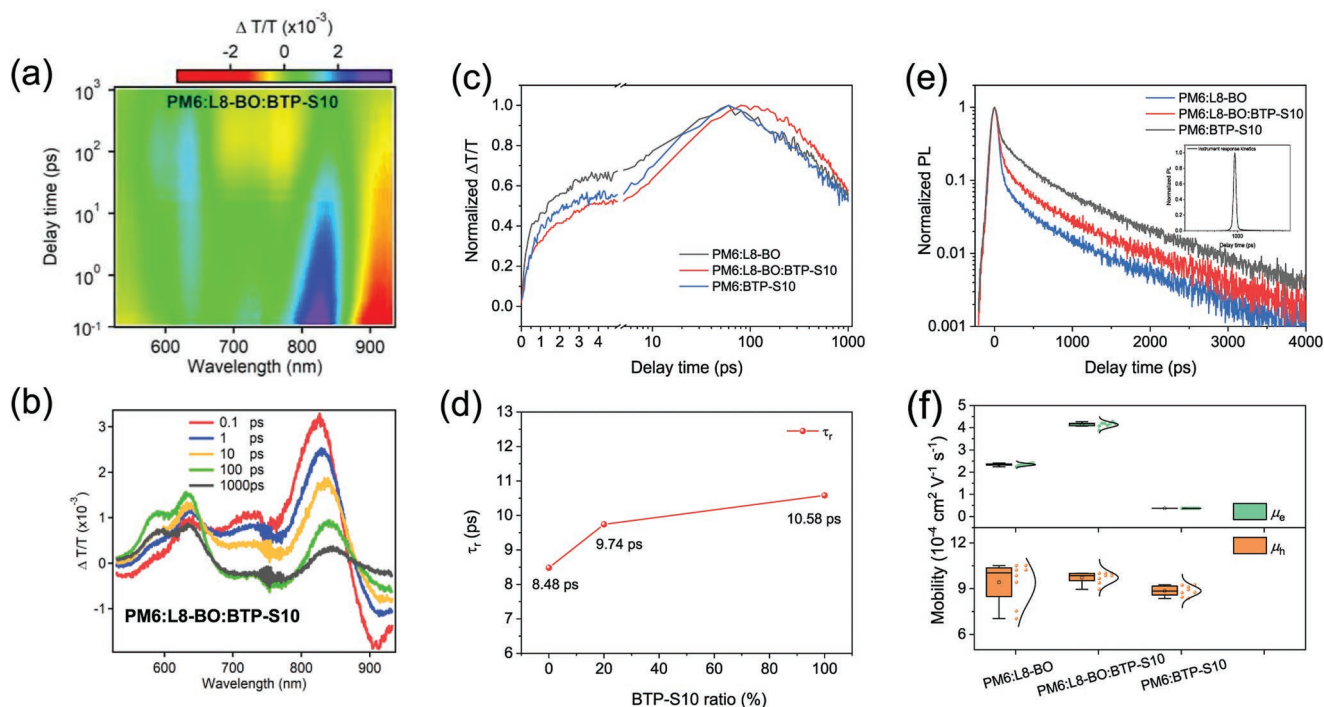


Figure 4. a) Color plot of TA spectra of PM6:L8-BO:BTP-S10 blend films under 800 nm excitation. b) The corresponding TA spectra. c) Hole transfer kinetics in three blend films. d) Comparisons of τ_h of different blends. e) TRPL of PM6:L8-BO, PM6:L8-BO:BTP-S10, and PM6:BTP-S10 thin films probed at 850–950 nm (illustrations: instrument response kinetics). f) Electron mobility and hole mobility comparisons of relevant blends (error bar is defined as the standard deviation, which is calculated from the statistics results of eight devices).

of TOPV is optimized, which contributes to J_{sc} and FF of ternary devices.

2.5. Film Morphology

The photoactive layer's top surface structure and aggregation properties were studied using atomic force microscopy (AFM). As shown in **Figure 5a**, the PM6:L8-BO film is smooth with a minor roughness (root-mean-square [RMS]) of 1.01 nm, due to the good compatibility between PM6 and L8-BO. In contrast, the surface of the PM6:BTP-S10 film is obviously rougher (RMS = 2.27 nm) than that of the PM6:L8-BO film, demonstrating the worse miscibility between PM6 and BTP-S10. For the ternary blend, the roughness increases to 1.16 nm with possibly a bit enlarged domain sizes, as a result of reduced miscibility between PM6 and L8-BO:BTP-S10. The corresponding AFM phase images are displayed in Figure S14, Supporting Information.

Further, the orientation and packing of molecules in the relevant films were explored by grazing wide-angle X-ray scattering (GIWAXS) characterization, as shown in Figure 5b–d and Figure S15, Supporting Information. For the neat acceptor films, L8-BO and BTP-S10 offer strong π - π stacking peaks ($\approx 1.72 \text{ \AA}^{-1}$, $d = 0.37 \text{ nm}$) in the out-of-plane (OOP) direction, while in the in-plane (IP) direction, both acceptors also have a strong lamellar peak ($\approx 0.39 \text{ \AA}^{-1}$, $d = 1.64 \text{ nm}$), representing both acceptors prefer a face-on orientation. The result of L8-BO:BTP-S10 blend resembles those observed in L8-BO, indicating the introduction of BTP-S10 will not destroy the crystal

structure of L8-BO. The D:A blend retains the packing properties of the polymer donor PM6 and acceptor molecules, and the ternary blend film is consistent with the trend of the two acceptor blends in terms of molecular packing orientation, which contribute to the enhanced charge transport properties of the ternary blend films, as shown in Table S4, Supporting Information.

3. Conclusion

In conclusion, we demonstrate an efficient ternary strategy to achieve a synergistic improvement of V_{oc} and J_{sc} via mixing two NFAs, that is, symmetric acceptor (L8-BO) and asymmetric acceptor (BTP-S10), with different terminals and alkyl side chains. It shows that the increase of V_{oc} in the TOPV is partly due to the lower radiative recombination loss that originated from the reduced degree of energy disorder, partly due to the reduced non-radiative recombination loss caused by the diminished ΔE_{LE-CT} and the higher luminescence efficiency in TOPV. Wetting coefficient value confirms that BTP-S10 locates at the interface of PM6:L8-BO in the ternary blend, offering extra exciton separation and charge transport channels. Exciton kinetics and morphological analysis indicate that the ternary blends maintain a high efficiency of exciton dissociation, obtain a longer exciton lifetime, and achieve the reduced charge recombination degree. The homogeneously mixed ternary films maintain good phase separation and dominant face-on orientation, thus promoting the charge transport capability in TOPV. The benefits in both charge transport and

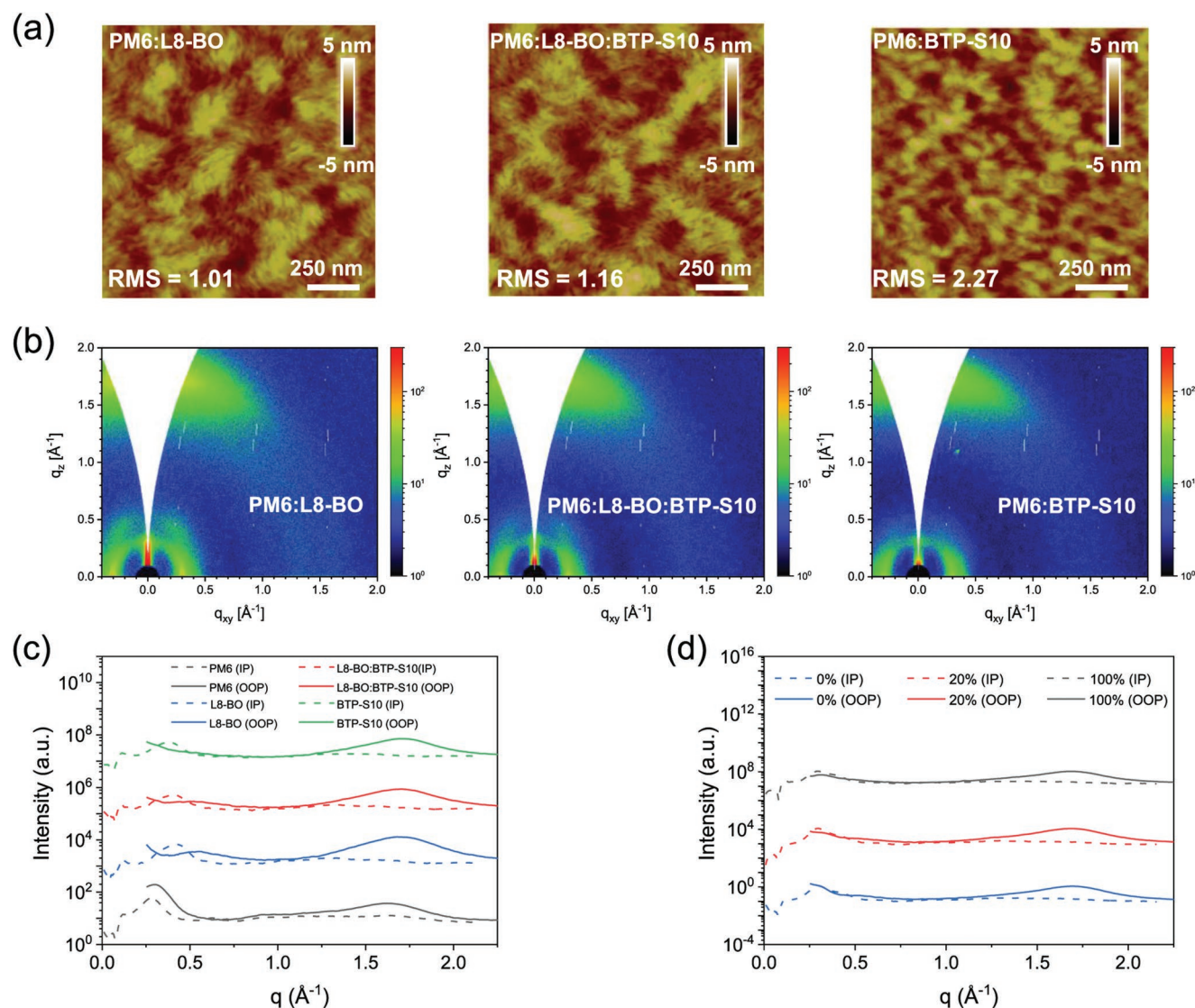


Figure 5. a) AFM height images of PM6:L8-BO, PM6:L8-BO:BTP-S10, and PM6:BTP-S10 blends. b) 2D GIWAXS images of PM6:L8-BO, PM6:L8-BO:BTP-S10, and PM6:BTP-S10 blend films. c,d) Intensity profiles of relevant films along the in-plane (dash lines) and out-of-plane (solid lines) directions.

charge recombination should be responsible for the increase of J_{sc} in the TOPV. Finally, all above privileges contribute to the achievement of a champion PCE of 19.26% for the TOPVs, which is currently one of the highest reported values of single-junction OPV.

Supporting Information

Supporting Information is available from the Wiley Online Library or from the author.

Acknowledgements

L.Z., S.L., and Y.L. contributed equally to this work. This work is supported by the National Natural Science Foundation of China (Nos.

21734008, 5212780017, 51803178, 61721005, 21971049), S&T Innovation 2025 Major Special Programme of Ningbo (No. 2018B10055), and the China Postdoctoral Science Foundation funded project (No. 2022M712737). L.Z. acknowledges the research start-up fund from Hangzhou Normal University (No. 2021QDL066). S.Y. acknowledges the financial support from the “Ten-thousand Talents Plan” of Zhejiang Province (No. 2019R52040).

Conflict of Interest

The authors declare no conflict of interest.

Data Availability Statement

Research data are not shared.

Keywords

charge transfer state, energy loss, high efficiency, intermediary electron acceptor, ternary organic photovoltaics

Received: March 28, 2022

Revised: August 4, 2022

Published online: August 21, 2022

- [1] Y. Lin, J. Wang, Z.-G. Zhang, H. Bai, Y. Li, D. Zhu, X. Zhan, *Adv. Mater.* **2015**, *27*, 1170.
- [2] M. Zhang, X. Guo, W. Ma, H. Ade, J. Hou, *Adv. Mater.* **2015**, *27*, 4655.
- [3] J. Hou, O. Inganäs, R. H. Friend, F. Gao, *Nat. Mater.* **2018**, *17*, 119.
- [4] S. Li, L. Zhan, F. Liu, J. Ren, M. Shi, C.-Z. Li, T. P. Russell, H. Chen, *Adv. Mater.* **2018**, *30*, 1705208.
- [5] J. Yuan, Y. Zhang, L. Zhou, G. Zhang, H.-L. Yip, T.-K. Lau, X. Lu, C. Zhu, H. Peng, P. A. Johnson, M. Leclerc, Y. Cao, J. Ulanski, Y. Li, Y. Zou, *Joule* **2019**, *3*, 1140.
- [6] S. Liu, J. Yuan, W. Deng, M. Luo, Y. Xie, Q. Liang, Y. Zou, Z. He, H. Wu, Y. Cao, *Nat. Photonics* **2020**, *14*, 300.
- [7] T. Wang, G. Kupgan, J.-L. Brédas, *Trends Chem.* **2020**, *2*, 535.
- [8] S. Li, L. Zhan, N. Yao, X. Xia, Z. Chen, W. Yang, C. He, L. Zuo, M. Shi, H. Zhu, X. Lu, F. Zhang, H. Chen, *Nat. Commun.* **2021**, *12*, 4627.
- [9] L. Feng, J. Yuan, Z. Zhang, H. Peng, Z.-G. Zhang, S. Xu, Y. Liu, Y. Li, Y. Zou, *ACS Appl. Mater. Interfaces* **2017**, *9*, 31985.
- [10] L. Zhan, S. Li, T.-K. Lau, Y. Cui, X. Lu, M. Shi, C.-Z. Li, H. Li, J. Hou, H. Chen, *Energy Environ. Sci.* **2020**, *13*, 635.
- [11] F. Qin, L. Sun, H. Chen, Y. Liu, X. Lu, W. Wang, T. Liu, X. Dong, P. Jiang, Y. Jiang, L. Wang, Y. Zhou, *Adv. Mater.* **2021**, *33*, 2103017.
- [12] R. Sun, W. Wang, H. Yu, Z. Chen, X. Xia, H. Shen, J. Guo, M. Shi, Y. Zheng, Y. Wu, W. Yang, T. Wang, Q. Wu, Y. Yang, X. Lu, J. Xia, C. J. Brabec, H. Yan, Y. Li, J. Min, *Joule* **2021**, *5*, 1548.
- [13] Y. Wei, J. Yu, L. Qin, H. Chen, X. Wu, Z. Wei, X. Zhang, Z. Xiao, L. Ding, F. Gao, H. Huang, *Energy Environ. Sci.* **2021**, *14*, 2314.
- [14] L. Zhan, S. Li, X. Xia, Y. Li, X. Lu, L. Zuo, M. Shi, H. Chen, *Adv. Mater.* **2021**, *33*, 2007231.
- [15] L. Zhan, S. Li, Y. Li, R. Sun, J. Min, Z. Bi, W. Ma, Z. Chen, G. Zhou, H. Zhu, M. Shi, L. Zuo, H. Chen, *Joule* **2022**, *6*, 662.
- [16] H. Zhao, B. Lin, J. Xue, H. B. Naveed, C. Zhao, X. Zhou, K. Zhou, H. Wu, Y. Cai, D. Yun, Z. Tang, W. Ma, *Adv. Mater.* **2022**, *34*, 2105114.
- [17] Z. Zheng, J. Wang, P. Bi, J. Ren, Y. Wang, Y. Yang, X. Liu, S. Zhang, J. Hou, *Joule* **2022**, *6*, 171.
- [18] L. Zuo, S. B. Jo, Y. Li, Y. Meng, R. J. Stoddard, Y. Liu, F. Lin, X. Shi, F. Liu, H. W. Hillhouse, D. S. Ginger, H. Chen, A. K. Y. Jen, *Nat. Nanotechnol.* **2022**, *17*, 53.
- [19] P. Bi, S. Zhang, Z. Chen, Y. Xu, Y. Cui, T. Zhang, J. Ren, J. Qin, L. Hong, X. Hao, J. Hou, *Joule* **2021**, *5*, 2408.
- [20] K. Chong, X. Xu, H. Meng, J. Xue, L. Yu, W. Ma, Q. Peng, *Adv. Mater.* **2022**, *34*, 2109516.
- [21] Y. Cai, Y. Li, R. Wang, H. Wu, Z. Chen, J. Zhang, Z. Ma, X. Hao, Y. Zhao, C. Zhang, F. Huang, Y. Sun, *Adv. Mater.* **2021**, *33*, 2101733.
- [22] Y. Zeng, D. Li, Z. Xiao, H. Wu, Z. Chen, T. Hao, S. Xiong, Z. Ma, H. Zhu, L. Ding, Q. Bao, *Adv. Energy Mater.* **2021**, *11*, 2101338.
- [23] Z. Du, X. Bao, Y. Li, D. Liu, J. Wang, C. Yang, R. Wimmer, L. W. Städe, R. Yang, D. Yu, *Adv. Energy Mater.* **2018**, *8*, 1701471.
- [24] S. Li, L. Zhan, C. Sun, H. Zhu, G. Zhou, W. Yang, M. Shi, C.-Z. Li, J. Hou, Y. Li, H. Chen, *J. Am. Chem. Soc.* **2019**, *141*, 3073.
- [25] J. Zhang, W. Liu, G. Zhou, Y. Yi, S. Xu, F. Liu, H. Zhu, X. Zhu, *Adv. Energy Mater.* **2020**, *10*, 1903298.
- [26] T. A. Dela Peña, J. I. Khan, N. Chaturvedi, R. Ma, Z. Xing, J. Gorenflot, A. Sharma, F. L. Ng, D. Baran, H. Yan, F. Laquai, K. S. Wong, *ACS Energy Lett.* **2021**, *6*, 3408.
- [27] Y. Li, Y. Guo, Z. Chen, L. Zhan, C. He, Z. Bi, N. Yao, S. Li, G. Zhou, Y. Yi, Y. Yang, H. Zhu, W. Ma, F. Gao, F. Zhang, L. Zuo, H. Chen, *Energy Environ. Sci.* **2022**, *15*, 855.
- [28] Q. Liu, Y. Wang, J. Fang, H. Liu, L. Zhu, X. Guo, M. Gao, Z. Tang, L. Ye, F. Liu, M. Zhang, Y. Li, *Nano Energy* **2021**, *85*, 105963.
- [29] J. Yan, E. Rezasoltani, M. Azzouzi, F. Eisner, J. Nelson, *Nat. Commun.* **2021**, *12*, 3642.
- [30] B.-H. Jiang, Y.-J. Peng, Y.-W. Su, J.-F. Chang, C.-C. Chueh, T.-S. Shieh, C.-I. Huang, C.-P. Chen, *Chem. Eng. J.* **2022**, *431*, 133950.
- [31] G. Yu, J. Gao, J. C. Hummelen, F. Wudl, A. J. Heeger, *Science* **1995**, *270*, 1789.
- [32] J. Lee, K. Vandewal, S. R. Yost, M. E. Bahlke, L. Goris, M. A. Baldo, J. V. Manca, T. V. Voorhis, *J. Am. Chem. Soc.* **2010**, *132*, 11878.
- [33] T. Linderl, T. Zechel, A. Hofmann, T. Sato, K. Shimizu, H. Ishii, W. Brütting, *Phys. Rev. Appl.* **2020**, *13*, 024061.
- [34] M. Zhang, L. Zhu, T. Hao, G. Zhou, C. Qiu, Z. Zhao, N. Hartmann, B. Xiao, Y. Zou, W. Feng, H. Zhu, M. Zhang, Y. Zhang, Y. Li, T. P. Russell, F. Liu, *Adv. Mater.* **2021**, *33*, 2007177.
- [35] N. Y. Doumon, L. Yang, F. Rosei, *Nano Energy* **2022**, *94*, 106915.
- [36] X.-K. Chen, D. Qian, Y. Wang, T. Kirchartz, W. Tress, H. Yao, J. Yuan, M. Hülsbeck, M. Zhang, Y. Zou, Y. Sun, Y. Li, J. Hou, O. Inganäs, V. Coropceanu, J.-L. Bredas, F. Gao, *Nat. Energy* **2021**, *6*, 799.
- [37] X. Du, Y. Yuan, L. Zhou, H. Lin, C. Zheng, J. Luo, Z. Chen, S. Tao, L.-S. Liao, *Adv. Funct. Mater.* **2020**, *30*, 1909837.
- [38] X. Xu, Y. Li, Q. Peng, *Adv. Mater.* **2022**, <https://doi.org/10.1002/adma.202107476>, 2107476.
- [39] J. Gao, W. Gao, X. Ma, Z. Hu, C. Xu, X. Wang, Q. An, C. Yang, X. Zhang, F. Zhang, *Energy Environ. Sci.* **2020**, *13*, 958.
- [40] H. Sun, B. Liu, Y. Ma, J.-W. Lee, J. Yang, J. Wang, Y. Li, B. Li, K. Feng, Y. Shi, B. Zhang, D. Han, H. Meng, L. Niu, B. J. Kim, Q. Zheng, X. Guo, *Adv. Mater.* **2021**, *33*, 2102635.
- [41] Y. Ni, X. Liu, Y. Liu, Z. Feng, D. Tu, X. Guo, C. Li, *ACS Appl. Mater. Interfaces* **2022**, *14*, 12461.
- [42] C. Li, J. Zhou, J. Song, J. Xu, H. Zhang, X. Zhang, J. Guo, L. Zhu, D. Wei, G. Han, J. Min, Y. Zhang, Z. Xie, Y. Yi, H. Yan, F. Gao, F. Liu, Y. Sun, *Nat. Energy* **2021**, *6*, 605.
- [43] S. Li, L. Zhan, Y. Jin, G. Zhou, T.-K. Lau, R. Qin, M. Shi, C.-Z. Li, H. Zhu, X. Lu, F. Zhang, H. Chen, *Adv. Mater.* **2020**, *32*, 2001160.
- [44] L. Ye, W. Zhao, S. Li, S. Mukherjee, J. H. Carpenter, O. Awartani, X. Jiao, J. Hou, H. Ade, *Adv. Energy Mater.* **2017**, *7*, 1602000.
- [45] L. Ye, H. Hu, M. Ghasemi, T. Wang, B. A. Collins, J.-H. Kim, K. Jiang, J. H. Carpenter, H. Li, Z. Li, T. McAfee, J. Zhao, X. Chen, J. L. Y. Lai, T. Ma, J.-L. Bredas, H. Yan, H. Ade, *Nat. Mater.* **2018**, *17*, 253.
- [46] M. Ghasemi, N. Balar, Z. Peng, H. Hu, Y. Qin, T. Kim, J. J. Rech, M. Bidwell, W. Mask, I. McCulloch, W. You, A. Amassian, C. Risko, B. T. O'Connor, H. Ade, *Nat. Mater.* **2021**, *20*, 525.
- [47] M. Sumita, K. Sakata, S. Asai, K. Miyasaka, H. Nakagawa, *Polym. Bull.* **1991**, *25*, 265.
- [48] M. Jiang, H. Bai, H. Zhi, L. Yan, H. Y. Woo, L. Tong, J. Wang, F. Zhang, Q. An, *Energy Environ. Sci.* **2021**, *14*, 3945.
- [49] J. Yao, T. Kirchartz, M. S. Vezie, M. A. Faist, W. Gong, Z. He, H. Wu, J. Troughton, T. Watson, D. Bryant, J. Nelson, *Phys. Rev. Appl.* **2015**, *4*, 014020.
- [50] U. Rau, *Phys. Rev. B: Condens. Matter* **2007**, *76*, 085303.
- [51] H. Xia, Y. Zhang, W. Deng, K. Liu, X. Xia, C.-J. Su, U.-S. Jeng, M. Zhang, J. Huang, J. Huang, C. Yan, W.-Y. Wong, X. Lu, W. Zhu, G. Li, *Adv. Mater.* **2022**, *34*, 2107659.
- [52] R. A. Marcus, *J. Phys. Chem.* **1989**, *93*, 3078.

- [53] D. Qian, Z. Zheng, H. Yao, W. Tress, T. R. Hopper, S. Chen, S. Li, J. Liu, S. Chen, J. Zhang, X.-K. Liu, B. Gao, L. Ouyang, Y. Jin, G. Pozina, I. A. Buyanova, W. M. Chen, O. Inganäs, V. Coropceanu, J.-L. Bredas, H. Yan, J. Hou, F. Zhang, A. A. Bakulin, F. Gao, *Nat. Mater.* **2018**, *17*, 703.
- [54] V. Coropceanu, X.-K. Chen, T. Wang, Z. Zheng, J.-L. Brédas, *Nat. Rev. Mater.* **2019**, *4*, 689.
- [55] Y. Cai, Q. Li, G. Lu, H. S. Ryu, Y. Li, H. Jin, Z. Chen, Z. Tang, G. Lu, X. Hao, H. Y. Woo, C. Zhang, Y. Sun, *Nat. Commun.* **2022**, *13*, 2369.